

Spectral-Bias and Kernel-Task Alignment in Physically Informed Neural Networks

Inbar Seroussi* Asaf Miron † Zohar Ringel ‡

Abstract

Physically informed neural networks (PINNs) are a promising emerging method for solving differential equations. As in many other deep learning approaches, the choice of PINN design and training protocol requires careful craftsmanship. Here, we suggest a comprehensive theoretical framework that sheds light on this important problem. Leveraging an equivalence between infinitely over-parameterized neural networks and Gaussian process regression (GPR), we derive an integro-differential equation that governs PINN prediction in the large data-set limit—the Neurally-Informed Equation (NIE). This equation augments the original one by a kernel term reflecting architecture choices and allows quantifying implicit bias induced by the network via a spectral decomposition of the source term in the original differential equation.

Introduction

Deep neural networks (DNNs) are revolutionizing a myriad of data-intensive disciplines [2, 20, 23], offering optimization-based alternatives to handcrafted algorithms. The recent “physics-informed neural network” (PINN) approach [39] trains DNNs to approximate solutions to partial differential equations (PDEs) by directly introducing the PDE and boundary/initial conditions into the loss function, effectively enforcing the PDE on a set of collocation points in the domain of interest. Its promise has attracted broad attention [3, 3, 6–8, 13, 15, 17, 19, 21, 29, 33, 38, 42]. While classical methods currently still outperform PINNs in various settings [12, 30], the excitement regarding PINNs based on several clear benefits: Their inherent support of exact automatic differentiation (AD) and corresponding mesh-free nature, which altogether bypasses discretization, truncation and dispersion errors, the promise of breaking the curse of dimensionality [12], as well as their ability to integrate data, either to improve training or to solve inverse problems, where noisy experimental data is supplied as input for calibrating PDE parameters [21].

*Department of Applied Mathematics, School of Mathematical Sciences, Tel Aviv University, Tel Aviv 69978, Israel

†Hebrew University, Racah Institute of Physics, Jerusalem, 9190401, Israel

‡Hebrew University, Racah Institute of Physics, Jerusalem, 9190401, Israel

Despite the rapid improvement of PINN-based algorithms, a theoretical understanding detailing just how PINNs train, why training sometimes fails [22,32], and how PINN architecture interacts with the PDE to affect performance is very limited. The first steps towards such a theoretical exploration of PINNs were carried out in [46,47]. These efforts made use of the fact that, in a suitable infinite over-parametrization limit, almost all DNNs effectively behave as Gaussian Processes (GPs), amounting to Bayesian inference with a Gaussian prior over function space [11,18,36]. The neural tangent kernel (NTK), a particular GP limit, was shown to be applicable to PINN settings and was used to propose algorithmic methods to engineer PINN parameters in order to circumvent spectral bias. Still, these efforts did not shed light on the relation between DNN architecture, the PDE type, and performance.

Recent years have seen remarkable progress in our understanding of GP limits, corrections to these limits [14,16,24,34,35,45], and their practical implications [1,26,49]. For supervised learning tasks, including real-world ones, it was shown that kernel-task alignment or spectral bias [4,5] is strongly predictive of DNN performance. Specifically, diagonalizing the GP kernel on the measure induced by the dataset leads to a series of features and eigenvalues. Those features with high eigenvalues can be learned with the least amount of effort. Furthermore, closely related approaches have led to practical recipes on how to scale up hyperparameters [49] and predict the scaling of performance with the number of parameters and data points [1,26].

In this paper, we extend the above notions of spectral bias and kernel-task alignment and provide a theoretical framework for PINNs. Our main result is a derivation of the neurally-informed equation, an integro-differential equation that approximates PINN predictions. This equation fleshes out tangible links between the DNN’s kernel, the original differential equation, and PINN’s prediction. In the limit of an infinite dataset, the neurally-informed equation reduces to the original equation, yet for large but finite datasets it captures the difference between the exact solution and the PINN solution. For example, it demonstrates how PINN performance improves when the source term resides in the large eigenvalue sector of the operator given by the kernel conjugated with the differential operator of the equation.

1 The model

Consider the following well-posed partial differential equation (PDE) defined on a closed bounded domain, $\Omega \subseteq \mathbb{R}^d$

$$\begin{aligned} L[f](\mathbf{x}) &= \phi(\mathbf{x}) & \mathbf{x} \in \Omega \\ f(\mathbf{x}) &= g(\mathbf{x}) & \mathbf{x} \in \partial\Omega \end{aligned} \tag{1}$$

where L is a differential operator and $f : \Omega \rightarrow \mathbb{R}$ is the PDE’s unknown solution with $\mathbf{x} \in \mathbb{R}^d$. The functions $\phi : \Omega \rightarrow \mathbb{R}$, $g : \partial\Omega \rightarrow \mathbb{R}$ are the PDE’s respective source term and initial/boundary conditions. In what follows, we use bold font to denote vectors.

In the PINN setting, we are given sample data (collocation points) $\mathcal{D}_n = \{f_\mu, \mathbf{x}_\mu\}_{\mu=1}^n$, such that $f_\mu = f(\mathbf{x}_\mu)$, where $n = n_{\partial\Omega} + n_\Omega$ and $n_\Omega, n_{\partial\Omega}$ denote

the number of data points in the domain’s bulk and on its boundary. We define the DNN estimator $\hat{f}_\theta : \Omega \rightarrow \mathbb{R}$ of the solution f , where θ are the network parameters. To train this DNN the following loss function is minimized

$$\mathcal{L} = \frac{1}{\sigma_\Omega^2} \sum_{\mu=1}^{n_\Omega} \left(L[\hat{f}_\theta](\mathbf{x}_\mu) - \phi(\mathbf{x}_\mu) \right)^2 + \frac{1}{\sigma_{\partial\Omega}^2} \sum_{\nu=1}^{n_{\partial\Omega}} \left(\hat{f}_\theta(\mathbf{x}_\nu) - g(\mathbf{x}_\nu) \right)^2, \quad (2)$$

where σ_Ω^2 , and $\sigma_{\partial\Omega}^2$ are some positive tunable constants. Obtaining analytical solutions to this optimization problem is obviously difficult. One analysis approach, which proved useful in the context of supervised learning, is to consider the limit of infinitely wide neural networks. Here, several simplifications arise, allowing one to map the problem to Bayesian Inference with Gaussian Processes (GPR) [18, 24, 28, 34].

Following this equivalence, one finds that the distribution of DNN outputs (f) of DNNs trained with full batch gradient descent, a small learning rate, and white noise ($\sigma^2 = 1$) with variance one added to gradients is given by

$$p(f|X_n) = e^{-\mathcal{S}[f|X_n]} / \mathcal{Z}(X_n), \quad (3)$$

with \mathcal{S} , called the “action”, given by:

$$\begin{aligned} \mathcal{S}[f|X_n] &= \frac{1}{2\sigma_\Omega^2} \sum_{\mu=1}^{n_\Omega} (L[f](\mathbf{x}_\mu) - \phi(\mathbf{x}_\mu))^2 \\ &+ \frac{1}{2\sigma_{\partial\Omega}^2} \sum_{\nu=1}^{n_{\partial\Omega}} (f(\mathbf{x}_\nu) - g(\mathbf{x}_\nu))^2 + \frac{1}{2} \sum_{\mu=0}^n \sum_{\nu=0}^n f_\mu [K^{-1}]_{\mu\nu} f_\nu. \end{aligned} \quad (4)$$

with the kernel K being the Gaussian process prior to the function, f . Here X_n denotes the set of collocation points $\{\mathbf{x}_\mu\}_{\mu=1}^{n_\Omega}$ and $\mathcal{Z}(X_n) = \int df e^{-\mathcal{S}[f|X_n]}$, called the “partition function”, plays the role of the distribution’s normalization. The first two terms in the action are associated with the loss function, and the last term is the GP prior. Note that, if the variance of the additive noise to the weights during the optimization is $\sigma^2 \neq 1$, then $\sigma_\Omega^2 \rightarrow \sigma_\Omega^2 \sigma^2$ and $\sigma_{\partial\Omega}^2 \rightarrow \sigma_{\partial\Omega}^2 \sigma^2$. Therefore, these constants, σ_Ω^2 , and $\sigma_{\partial\Omega}^2$ reflect Gaussian uncertainty on the measurement of how well $L[\hat{f}_\theta] = \phi$ and $\hat{f}_\theta = g$, respectively. The third term reflects the prior induced by an infinitely wide DNN with random weights under which, by the central limit theorem [18], the predictor $\hat{f}_\theta(\mathbf{x}_\mu)$ is a Gaussian process with kernel K . Finally, we extend the sample index by adding $\mu = 0$ to denote the test point \mathbf{x}_* at which we evaluate the estimator. Our goal here is to provide an approximate yet more insightful analytical prediction on $f(\mathbf{x}_*)$ where the average is taken first w.r.t to $p(f|X_n)$ and then with respect to all draws of X_n from a dataset measure $d\mu_{\mathbf{x}}$.

2 Results

Here we outline our main results. Further details on their derivations are found in the appendix.

2.1 The Neurally-Informed Equation (NIE)

Performing calculus of variations on the above action (or, equivalently, obtaining the Euler-Lagrange equations), requires care following the presence of both bulk and boundary integrals in the action. The resulting analysis leads to an integro-differential equation that we refer to as the neurally-informed equation. To illustrate, consider the general linear d -dimensional differential operator of order s , L . We remark that our formalism is general and can be applied to a nonlinear operator as well, by solving the variational problem defined by the nonlinear energy functional defined in Appendix B.1. For this choice of L , given that the kernel prior K is inevitable, we find the following Neurally-Informed Equation (NIE) for $f_0 : \Omega \rightarrow \mathbb{R}$, this equation is one of our main results,

$$f_0(\mathbf{x}) + \eta_\Omega \int_\Omega (Lf_0(\mathbf{y}) - \phi(\mathbf{y})) [LK](\mathbf{y}, \mathbf{x}) d\mathbf{y} + \eta_{\partial\Omega} \int_{\partial\Omega} (f_0(\mathbf{y}) - g(\mathbf{y})) K(\mathbf{x}, \mathbf{y}) d\mathbf{y} = 0 \quad (5)$$

where $\eta_\Omega = \frac{n_\Omega}{\sigma_\Omega^2}$, and $\eta_{\partial\Omega} = \frac{n_{\partial\Omega}}{\sigma_{\partial\Omega}^2}$. Here we have denoted integration w.r.t. the boundary and bulk measures as $\int_{\partial\Omega}$ and \int_Ω respectively. For simplicity, we take the distribution of points to be uniform both on the boundary, $1/|\partial\Omega|$, and on the bulk, $1/|\Omega|$ [39]. We further note that the above equation is obtained by applying variational calculus to an energy functional which is a leading order expansion in $[L[f](\mathbf{x}) - \phi(\mathbf{x})]^2 / \sigma_\Omega^2$ and $[f(\mathbf{x}) - g(\mathbf{x})]^2 / \sigma_{\partial\Omega}^2$. As such, it is valid when the mean training error is small compared to the observation noise. Perturbative corrections to this limit could be readily obtained using the formalism outlined in the appendix subsection B.1 (see also Ref. [5]).

Solving the neurally-informed equation yields the PINN prediction averaged over DNN ensembles and draws of X_n . In the limit of large n_Ω and $n_{\partial\Omega}$, the first $f_0(\mathbf{x})$ term is negligible and, at least for sufficiently smooth and non-singular kernels, one finds that the desired solution of the differential equation also satisfies this equation, i.e. f_0 is also satisfying $(Lf_0(\mathbf{x}) - \phi(\mathbf{x})) = 0$ for $\mathbf{x} \in \Omega$ and $f_0(\mathbf{x}) - g(\mathbf{x}) = 0$ for $\mathbf{x} \in \partial\Omega$. For finite $n_\Omega, n_{\partial\Omega}$, the spectral bias induced by the kernel starts playing a role. Next, we demonstrate our formalism with a simple toy example.

2.2 Toy example

To demonstrate the applicability of our approach, let us consider the following toy example: a system on the half-infinite one-dimensional interval $\Omega = [0, \infty)$, with a differential operator $L = \partial_x$ $g(x=0) = g_0$, and boundary condition $\phi(x) = 0$. Let us consider the following random neural network acting on a one-dimensional input x ,

$$f(x) = \sum_{c=1}^C a_c \cos(w_c x) \quad (6)$$

with $a_c \sim N(0, 1/(C\sqrt{2\pi l^2}))$ and $w_c \sim N(0, 1/l^2)$. As shown in Appendix C this network at the infinite width limit ($C \rightarrow \infty$) generate the following kernel,

$$K(x, x') = \frac{1}{2\sqrt{2\pi l^2}} \left(e^{-\frac{|x-x'|^2}{2l^2}} + e^{-\frac{|x+x'|^2}{2l^2}} \right). \quad (7)$$

The corresponding neurally-informed equation is given by

$$\int_0^\infty dy [K^{-1}(x, y) - \eta_\Omega \delta(x-y) \partial_y^2] f(y) = -\delta(x) [\eta_{\partial\Omega}(f(0) - g_0) - \eta_\Omega \partial_x f(0)] \quad (8)$$

where we have acted on the equation with $K^{-1}(x, y)$, defined such that

$$\int dy K^{-1}(x, y) K(y, z) = \delta(x - z).$$

To solve this equation, we first focus on inverting the operator $(K^{-1} + \eta_\Omega \partial_x^2)$ on the left-hand side of Eq. (6). To this end, we employ the following orthonormal basis functions for the positive half-interval,

$$\langle x | k \rangle = \frac{\sqrt{2}}{\sqrt{\pi}} \cos(kx) = \frac{1}{\sqrt{2\pi}} (e^{ikx} + e^{-ikx}). \quad (9)$$

where we adopt here a bra-ket notation, the bra $\langle x |$ denotes the position basis with the label x which extends over all points on the positive half line, and the ket $|k\rangle = \int_0^\infty dx \frac{e^{ixk}|x\rangle}{\sqrt{2\pi}}$. Transforming the bulk operator to this “ k -space” basis, i.e.

$$\langle k | (K^{-1} - \eta_\Omega \delta(x-y) \partial_y^2) | k' \rangle = \delta(k - k') \left(e^{+(kl)^2/2} + \eta_\Omega k^2 \right), \quad (10)$$

yields the following expression for the inverse operator (Green’s function)

$$G(x, x') = \frac{1}{\pi} \int_{-\infty}^{+\infty} dk \cos(kx) \cos(kx') \left(e^{+(kl)^2/2} + \eta_\Omega k^2 \right)^{-1}. \quad (11)$$

This integral can either be evaluated numerically or via contour integration. Taking the latter approach reveals an infinite set of simple poles. However, as $|x - x'|$ grows and/or for very large η_Ω , we find numerically that a single pole dominates the integral and yields $G(x, x') \approx \frac{\kappa}{2} \left(e^{-\kappa|x-x'|} + e^{-\kappa|x+x'|} \right)$ where $\kappa = \frac{1}{\sqrt{l^2/2 + \eta_\Omega}}$ for $\kappa l \ll 1$. While this approximation can be systematically improved by accounting for additional poles, in the numerics presented below we have simply calculated this integral numerically. Further details of the above derivation are given in Appendix D.

Next, we write the neurally-informed equation in the following form

$$f(x') = \int dx G(x', x) \delta(x) (\eta_{\partial\Omega} [g_0 - f(0)] + \eta_\Omega [Lf](0)) \quad (12)$$

We next define $\Delta = \eta_{\partial\Omega}[g_0 - f(0)] + \eta_{\Omega}[Lf](0)$, such that $f(x) = G(x, 0)\Delta$. We can now obtain an equation for Δ via,

$$\Delta = \eta_{\partial\Omega}(g(0) - \Delta G(0, 0)), \quad (13)$$

where we used the fact $\partial_x G(0, 0) = 0$ (see Eq. (11)). Following this we get,

$$\begin{aligned} \Delta(1 + G(0, 0)\eta_{\partial\Omega}) &= \eta_{\partial\Omega}g_0 \\ \Delta &= \frac{\eta_{\partial\Omega}g_0}{1 + G(0, 0)\eta_{\partial\Omega}}, \end{aligned} \quad (14)$$

finally, we find

$$f(x \geq 0) = g_0 \frac{\eta_{\partial\Omega}}{1 + G(0, 0)\eta_{\partial\Omega}} G(x, 0). \quad (15)$$

We proceed with testing this numerically by comparing the above results with exact Gaussian Process Regression (GPR) (see Appendix A for more detail). We consider $L = 512, l = 1, g_0 = 2.5, \sigma_{\partial\Omega}^2 = 0.01$ and single boundary point ($n_{\partial\Omega} = 1$) and scan n_{Ω} while keeping the ratio $n_{\Omega}/\sigma_{\Omega}^2$ fixed, which means that the neurally-informed equation’s predictions remain invariant to n_{Ω} . In doing so, we are essentially maintaining the amount of “training information” by providing more data while making it noisier. Notably, we do not include any dataset averaging in the GPR numerics. Figure 1 shows the GPR prediction alongside our prediction as a function of the test point’s value x_* , for, $n_{\Omega} = \{128, 1024, 8192\}$. The figure exhibits an excellent match between theory and experiment, even at relatively small numbers of points, n_{Ω} .

2.3 Spectral bias and figure of merit

A central element in deep learning is finding the right DNN architecture for the task at hand. Infinite width limits simplify this process by embodying all of the architecture’s details, along with training details such as weight decay terms and gradient noise, in a concrete mathematical object, the kernel $K(\mathbf{x}, \mathbf{y})$. Qualitatively speaking, these kernels also reflect the useful traits of realistic finite-width DNNs and CNNs [36].

In the context of standard Gaussian Process Regression, the learnability of a particular target function may be analyzed by projection onto the eigenfunctions of the continuum kernel operator [4, 5, 48]. Specifically, the GPR prediction, averaged over the dataset distribution, essentially acts as a high-pass linear filter on these eigenfunctions. This kernel-spectrum-based filtering is what we refer to as spectral bias.

In Appendix E we show that a somewhat similar form of spectral bias occurs in PINNs. However rather than being based on the spectrum of $K(\mathbf{x}, \mathbf{y})$, the relevant spectrum ($\hat{\lambda}_k$) and eigenfunctions ($\varphi_k(\mathbf{x})$) are those obtained by the following diagonalization procedure

$$\begin{aligned} \hat{K}_{\mathbf{x}\mathbf{y}} &= K(\mathbf{x}, \mathbf{y}) - \int_{\partial\Omega} \int_{\partial\Omega} K(\mathbf{x}, \mathbf{z}_1)[K + \eta_{\partial\Omega}^{-1}]^{-1}(\mathbf{z}_1, \mathbf{z}_2)K(\mathbf{z}_2, \mathbf{y})d\mathbf{z}_1d\mathbf{z}_2 \\ \int_{\Omega} [L\hat{K}L^\dagger](\mathbf{x}, \mathbf{y})\varphi_k(\mathbf{y}) &= \hat{\lambda}_k\varphi_k(\mathbf{x})d\mathbf{x} \end{aligned} \quad (16)$$

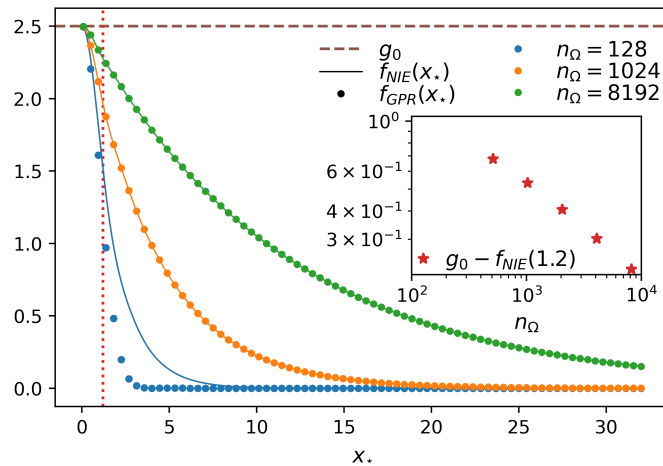


Figure 1: The GPR solution $f_{GPR}(x_*)$ (dots) and the neurally-informed equation prediction $f_{NIE}(x_*)$ (solid curves) versus x_* for three values of the number of bulk training points n_Ω . Here g_0 (dashed brown curve) denotes the value of the boundary condition at $x_* = 0$ and, in the toy example, the exact solution for all $x_* \in \mathbb{R}^+$. We set $L = 2^9 = 512$, $\sigma_\Omega^2 = 2^{-3} = 0.125$, $\ell^2 = 1$, $n_{\partial\Omega} = 1$ and $\sigma_{\partial\Omega}^2 = 2^{-6}/n_\Omega$, such that both η 's vary with n_Ω by the same proportion. The vertical dotted red line at $x_* = 1.2$ is discussed next in the inset. Inset: The difference $g_0 - f_{NIE}(x_* = 1.2)$ versus n_Ω becomes a linear function in log-log scale (red stars). This suggests a power-law scaling, which indicates that the difference vanishes as $n_\Omega \rightarrow \infty$.

where \hat{K} coincides with the dataset-averaged posterior covariance, given that one introduces only boundary points and fixes them to zero [5], $L\hat{K}L^\dagger = L_x L_y K(\mathbf{x}, \mathbf{y})$ where L_* is the differential operator acting on the variable $*$ = $\{x, y\}$, and the inverse of $[K + \eta_{\partial\Omega}^{-1}]$ is calculated w.r.t. the boundary measure. We note in passing that for small $\eta_{\partial\Omega}$, or if the boundary is a set of isolated points, \hat{K} can be expressed straightforwardly (see Appendix E). Next, we find that the discrepancy between $L[f]$ and ϕ is given by a low-pass filter on a boundary-augmented source term ($\hat{\phi}$), specifically

$$\begin{aligned} L[f](\mathbf{x}) - \phi(\mathbf{x}) &= \sum_k \frac{1}{1 + \hat{\lambda}_k \eta_{\partial\Omega}} c_k \varphi_k(\mathbf{x}) \\ \hat{\phi}(\mathbf{x}) &= \phi(\mathbf{x}) + \eta_{\partial\Omega} \int_{\partial\Omega} [L\hat{K}](\mathbf{x}, \mathbf{z}) g(\mathbf{z}) d\mathbf{z} \\ \hat{\phi}(\mathbf{x}) &= \sum_k c_k \varphi_k(\mathbf{x}). \end{aligned} \tag{17}$$

A simpler result, with no boundary term, is obtained by taking $\eta_{\partial\Omega} \rightarrow 0$, in which case $\phi(\mathbf{x}) = \hat{\phi}(\mathbf{x})$ and $\hat{K} = K$. Note that, the result of a classical GP regression problem is recovered from the above equation by taking the identity operator L , no boundary points, and taking ϕ to be the target.

The spectral bias presented in Eq. (17) is one of the key results of this work. It shows that smaller discrepancies are achieved when the augmented source term ($\hat{\phi}(\mathbf{x})$) lays in a high eigenvalues sector of $L\hat{K}L^\dagger$. Furthermore, the spectral components of $\phi(\mathbf{x})$ supported on $\hat{\lambda}_k \ll \eta_{\partial\Omega}^{-1} = \sigma_{\Omega}^2/n_{\Omega}$ are effectively ignored or projected out by the PINN. This suggests the following figure of merit measuring the overlap of the discrepancy with the augment source term, namely,

$$Q_n[\phi, g] \equiv \frac{\int_{\Omega} \hat{\phi}(\mathbf{x}) [L[f](\mathbf{x}) - \phi(\mathbf{x})] d\mathbf{x}}{\int_{\Omega} |\hat{\phi}(\mathbf{x})|^2 d\mathbf{x}} = \frac{\sum_k \frac{|c_k|^2}{1 + \hat{\lambda}_k \eta_{\partial\Omega}}}{\sum_k |c_k|^2} = \eta_{\partial\Omega}^{-1} \frac{\|\hat{\phi}\|_{\hat{K} + \eta_{\partial\Omega}^{-1}}^2}{\int_{\Omega} |\hat{\phi}(\mathbf{x})|^2 d\mathbf{x}} \tag{18}$$

where $\|\hat{\phi}\|_{\hat{K} + \eta_{\partial\Omega}^{-1}}^2$ is the RKHS norm of $\hat{\phi}$ with respect to the kernel $\hat{K} + \eta_{\partial\Omega}^{-1}$.

3 Discussion

In this work, we laid out an analytical framework for studying infinitely wide PINNs. By mapping the latter to Gaussian Processes and leveraging tools from statistical mechanics, we provided a concrete analytical formula for their average prediction, in the form of an integro-differential equation (the neurally-informed equation). Our formalism allows us to quantify spectral bias in PINN prediction and provides concrete figures of merit for kernel-task alignment.

Our framework may also help illuminate the reported difficulty of applying the standard PINN architecture to nonlinear hyperbolic partial differential equations [10, 25, 41]. In such equations, which include the inviscid Burgers' equation, the shallow-water equations, and the compressible Euler equations, discontinuous shock-wave solutions may appear at finite times, even for smooth

initial conditions. Spectral bias, which typically favors smooth functions, may explain some of the issues here. Another option is to generalize our approach to the recently introduced weak PINNs architectures [9, 31, 43, 44].

An additional exciting direction would be to apply our formalism to inverse problems [39], i.e. cases in which the coefficients of the equation are not known and are learned via a neural network. In this case, one could derive a neurally-informed equation coupled to algebraic equations governing the unknown coefficients.

Finite width effects are also relevant here and can be incorporated into our formalism using the methods of Refs. [24, 45]. Indeed, many authors report strong finite-width effects in the form of local minima in the training loss. Spectral bias affects the magnitude of finite width effects, and therefore the scale of width for which GP mappings become adequate. As GP limit of DNN exhibits no harmful local minima, this can help assess the resources needed to avoid such training issues.

Generally speaking, making predictions on DNN learning curves requires detailed knowledge of the high-dimensional input data distribution. Even for a fixed kernel, this distribution has a strong effect on the kernel eigenvalues and hence on what can be learned efficiently. Conveniently, for PINNs, this considerable obstacle is largely avoided as the data distributions are typically low dimensional. Furthermore, qualitative properties of the target function (i.e. the desired PDE solution) are often available. We thus find it plausible that spectral bias would lend itself to improve real-world PINN and provide guarantees on their performance.

A Gaussian Process Regression (GPR) formula

Focusing on linear insertable operators, and taking the prior on f to be a Gaussian process (GP) with kernel, K . As shown in Ref. [40], or in Ref. [37] section 14.3.3 for Laplacian operator, the average of $f(\mathbf{x}_*)$ under the multivariate Gaussian distribution in Eq. 4 is given by

$$\langle f_* \rangle_{P(f|X_n)} = \vec{k}^T (K_{\text{PINN}} + \tilde{\mathbb{I}})^{-1} \mathbf{y}, \quad (19)$$

where

$$\mathbf{y} = (\phi, \mathbf{g})^T, \quad (20)$$

the GP kernel is divided into blocks,

$$K = \begin{bmatrix} K(X_{n_\Omega}, X_{n_\Omega}) & K(X_{n_{\partial\Omega}}, X_{n_\Omega}) \\ K(X_{n_{\partial\Omega}}, X_{n_\Omega}) & K(X_{n_{\partial\Omega}}, X_{n_{\partial\Omega}}) \end{bmatrix} = \begin{bmatrix} K_{\Omega\Omega} & K_{\partial\Omega\Omega} \\ K_{\Omega\partial\Omega} & K_{\partial\Omega\partial\Omega} \end{bmatrix}, \quad (21)$$

where $X_{n_\Omega}, X_{n_{\partial\Omega}}$ are the data-points on the domain, Ω and on the boundary, $\partial\Omega$, respectively. We also define

$$\tilde{\mathbb{I}} = \begin{pmatrix} \sigma_\Omega^2 \mathbb{I} & 0 \\ 0 & \sigma_{\partial\Omega}^2 \mathbb{I} \end{pmatrix}. \quad (22)$$

where

$$K_{\text{PINN}} = \begin{pmatrix} LK_{\Omega,\Omega}L^\dagger & LK_{\Omega,\partial\Omega} \\ K_{\partial\Omega,\Omega}L^\dagger & K_{\partial\Omega,\partial\Omega} \end{pmatrix} \text{ and } \vec{k} = \begin{pmatrix} \vec{k}_\Omega L^\dagger \\ \vec{k}_{\partial\Omega} \end{pmatrix}, \quad (23)$$

where $(\vec{k}_\Omega)_\mu = K(\mathbf{x}_*, \mathbf{x}_{\mu \in [1, n_\Omega]})$ and $(\vec{k}_{\partial\Omega})_\mu = K(\mathbf{x}_*, \mathbf{x}_{\mu \in [n_\Omega+1, n_\Omega+n_{\partial\Omega}]})$. We denote by L the linear operator acting in the forward direction and L^\dagger the same operator acting ‘‘backwards’’ so that KL^\dagger is K acted upon by L on its second argument.

B Derivation of the Neurally-Informed Equation (NIE)

In this section, we derive our main result, the Neurally Informed Equation, Eq. (5) in the main text. We start by analyzing posterior distribution in function space and show that it can be written in terms of an effective energy function ‘‘action’’ for a general operator. This provides our first result. We then focus on a linear differential operator and use variational calculus to derive the NIE.

B.1 Derivation of the effective action

Using the Bayesian perspective, the posterior distribution in the function space can be written as follows:

$$\begin{aligned} p(\mathbf{f}|X_n) &= \mathcal{N}(\mathcal{L}(X_n), \sigma^2 = 1) p_0(f|X) \\ &= \prod_{\mu=1}^{n_\Omega} \mathcal{N}(L[f](\mathbf{x}_\mu) - \phi(\mathbf{x}_\mu), \sigma_\Omega^2) \prod_{\nu=1}^{n_{\partial\Omega}} \mathcal{N}(f(\mathbf{x}_\nu) - g(\mathbf{x}_\nu), \sigma_{\partial\Omega}^2) p_0(f|X), \end{aligned} \quad (24)$$

where $p_0(f|X_n) = \int d\boldsymbol{\theta} p(\boldsymbol{\theta}) \prod_{\mu} \delta\left(f(\mathbf{x}_{\mu}) - \hat{f}_{\boldsymbol{\theta}}(\mathbf{x}_{\mu})\right)$, and $\mathcal{L}(X_n)$ is the training loss in Eq. (2). Adopting a statistical physics viewpoint, we can write the posterior distribution as $p(\mathbf{f}|X_n) = \frac{1}{\mathcal{Z}[X_n]} e^{-\mathcal{S}[f|X_n]}$, where

$$\mathcal{S}[f|X_n] = \mathcal{S}_{\text{PDE}}[f|X_n] + \mathcal{S}_0[f|X_n] \quad (25)$$

where,

$$\mathcal{S}_{\text{PDE}}[f|X_n] = \mathcal{S}_{\Omega}[f|X_n] + \mathcal{S}_{\partial\Omega}[f|X_n] \quad (26)$$

$$= \frac{1}{2\sigma_{\Omega}^2} \sum_{\mu=1}^{n_{\Omega}} (L[f](\mathbf{x}_{\mu}) - \phi(\mathbf{x}_{\mu}))^2 + \frac{1}{2\sigma_{\partial\Omega}^2} \sum_{\nu=1}^{n_{\partial\Omega}} (f(\mathbf{x}_{\nu}) - g(\mathbf{x}_{\nu}))^2 \quad (27)$$

$$\mathcal{S}_0[f|X_n] = \frac{1}{2} \sum_{\mu=1}^n \sum_{\nu=1}^n f_{\mu} [K^{-1}]_{\mu\nu} f_{\nu} + \frac{1}{2} \log |K| + \frac{n}{2} (3 \log 2\pi + 2 \log \sigma_{\partial\Omega} \sigma_{\Omega}), \quad (28)$$

and $\mathcal{Z}[X_n] = \int e^{-\mathcal{S}[f|X_n]} df$ is the partition function.

To understand generalization, we are interested in computing ensemble averages over many data-sets. In the following, we use our freedom to choose the prior on the function to be on an infinite dataset, i.e. in the reproduction kernel Hilbert space (RKHS), with the kernel being the continuum version of Eq. (21). Utilizing a statistical mechanics approach, we want to compute the free energy, $\mathbb{E}_{\mathcal{D}_n} [\log \mathcal{Z}[X_n]]$ which can also be viewed as the generating function of the process. For this purpose, we employ the replica trick:

$$\mathbb{E}_{\mathcal{D}_n} [\log \mathcal{Z}[X_n]] = \lim_{p \rightarrow 0} \frac{\partial \log \mathbb{E}_{\mathcal{D}_n} [\mathcal{Z}^p[X_n]]}{\partial p}$$

where

$$\begin{aligned} \mathbb{E}_{\mathcal{D}_n} [\mathcal{Z}^p[X]] &= \mathbb{E}_{\mathcal{D}_n} \left[\int \prod_{\alpha}^p e^{-\mathcal{S}[f_{\alpha}|X_n]} df_{\alpha} \right] \\ &= \int \mathbb{E}_{\mathcal{D}_n} \left[e^{-\sum_{\alpha=1}^p \mathcal{S}_{\text{PDE}}[f_{\alpha}|X_n]} \right] \prod_{\alpha}^p p_0(f_{\alpha}) df_{\alpha} \\ &= \langle \mathbb{E}_{\mathcal{D}_n} \left[e^{-\sum_{\alpha=1}^p \mathcal{S}_{\text{PDE}}[f_{\alpha}|X_n]} \right] \rangle_{0,p} = \langle \left(\mathbb{E}_{\mathbf{x}} \left[e^{-\sum_{\alpha=1}^p \mathcal{S}_{\text{PDE}}[f_{\alpha}|\mathbf{x}]} \right] \right)^n \rangle_{0,p} \end{aligned} \quad (29)$$

where $\langle \dots \rangle_{0,p}$ denotes expectation over the p replicated prior distribution, $p_0(f)$. The above object is still hard to analyze. To make progress, we follow a similar approach as in [5, 27]. We transform into a ‘‘grand canonical’’ partition function, meaning that we treat the dataset size n as a random variable and average over it. The idea is that for a large enough data set size. The dominating term in the grad canonical partition function G_p can be used to estimate the free energy.

The grad canonical partition function,

$$\begin{aligned}
\bar{G}_p &= \mathbb{E}_n [\mathbb{E}_{\mathcal{D}_n} [\mathcal{Z}^p[X_n]]] \\
&= \left\langle \sum_{u_1=0}^{\infty} \frac{\bar{\eta}_{\Omega}^{u_1} e^{-\bar{\eta}_{\Omega}}}{u_1!} \mathbb{E}_{\mathcal{D}_{u_1}} \left[e^{-\sum_{\alpha=1}^p \mathcal{S}_{\Omega}[f_{\alpha}|X_{u_1}]} \right] \sum_{u_2=0}^{\infty} \frac{\bar{\eta}_{\partial\Omega}^{u_2} e^{-\bar{\eta}_{\partial\Omega}}}{u_2!} \mathbb{E}_{\mathcal{D}_{u_2}} \left[e^{-\sum_{\alpha=1}^p \mathcal{S}_{\partial\Omega}[f_{\alpha}|X_{u_2}]} \right] \right\rangle_{0,p} \\
&= \left\langle \sum_{u_1=0}^{\infty} \frac{\bar{\eta}_{\Omega}^{u_1} e^{-\bar{\eta}_{\Omega}}}{u_1!} \left(\mathbb{E}_{\mathbf{x}} \left[e^{-\sum_{\alpha=1}^p \mathcal{S}_{\Omega}[f_{\alpha}|\mathbf{x}]} \right] \right)^{u_1} \sum_{u_2=0}^{\infty} \frac{\bar{\eta}_{\partial\Omega}^{u_2} e^{-\bar{\eta}_{\partial\Omega}}}{u_2!} \left(\mathbb{E}_{\mathbf{x}} \left[e^{-\sum_{\alpha=1}^p \mathcal{S}_{\partial\Omega}[f_{\alpha}|\mathbf{x}]} \right] \right)^{u_2} \right\rangle_{0,p} \\
&= \int \prod_{\alpha}^p e^{-\bar{\eta} + \bar{\eta}_{\Omega} \mathbb{E}_{\mathbf{x}} \left[e^{-\sum_{\alpha=1}^p \mathcal{S}_{\Omega}[f_{\alpha}|\mathbf{x}]} \right] + \bar{\eta}_{\partial\Omega} \mathbb{E}_{\mathbf{x}} \left[e^{-\sum_{\alpha=1}^p \mathcal{S}_{\partial\Omega}[f_{\alpha}|\mathbf{x}]} \right]} p_0(f_{\alpha}) df_{\alpha} \\
&= \int e^{-\sum_{\alpha=1}^p \mathcal{S}_{\text{eff}}[f_{\alpha}]} \prod_{\alpha}^p \mathcal{Z}_{\alpha}^{-1} df_{\alpha} \quad (30)
\end{aligned}$$

where in the third transition, we assume that if the i th point is on the bulk then $\mathbf{x}_i \sim \mu_{\Omega}(\mathbf{x})$, otherwise, $\mathbf{x}_i \sim \mu_{\partial\Omega}(\mathbf{x})$ all points are independent. With a slight abuse of notation, we take $n_{\Omega} \sim \text{Pois}(\bar{\eta}_{\Omega})$, and $n_{\partial\Omega} \sim \text{Pois}(\bar{\eta}_{\partial\Omega})$ as independent random variables. We denote by $\bar{\eta} = \bar{\eta}_{\Omega} + \bar{\eta}_{\partial\Omega}$, where $\bar{\eta}_{\Omega}$ and $\bar{\eta}_{\partial\Omega}$ are the true deterministic number of points in the bulk and on the boundary, respectively. The effective action is then defined:

$$\begin{aligned}
\mathcal{S}_{\text{eff}}[f] &= \bar{\eta} - \bar{\eta}_{\Omega} \mathbb{E}_{\mathbf{x}} \left[e^{-\mathcal{S}_{\Omega}[f|\mathbf{x}]} \right] - \bar{\eta}_{\partial\Omega} \mathbb{E}_{\mathbf{x}} \left[e^{-\mathcal{S}_{\partial\Omega}[f|\mathbf{x}]} \right] \\
&\quad + \frac{1}{2} \int_{\Omega} \int_{\Omega} f(\mathbf{x}) [K^{-1}](\mathbf{x}, \mathbf{y}) f(\mathbf{y}) d\mathbf{y} d\mathbf{x}. \quad (31)
\end{aligned}$$

Next, Taylor expanding the above exponent, we obtain the following effective action in first-order,

$$\begin{aligned}
\mathcal{S}_{\text{eff}}[f] &= \bar{\eta}_{\Omega} \mathbb{E}_{\mathbf{x}} [\mathcal{S}_{\Omega}[f|\mathbf{x}]] - \bar{\eta}_{\partial\Omega} \mathbb{E}_{\mathbf{x}} [\mathcal{S}_{\partial\Omega}[f|\mathbf{x}]] \\
&\quad + \frac{1}{2} \int_{\Omega} \int_{\Omega} f(\mathbf{x}) [K^{-1}](\mathbf{x}, \mathbf{y}) f(\mathbf{y}) d\mathbf{x} d\mathbf{y} + O(\bar{\eta}^2/\sigma^4),
\end{aligned}$$

where $\sigma^2 = \sigma_{\Omega}^2 + \sigma_{\partial\Omega}^2$. Note that, the first-order action decouples the replica modes, which drastically simplifies the analysis. Taking higher-order corrections into account would lead to a tighter prediction. Figure 1 shows that the estimated output derived using the first-order action provides a good prediction for a large amount of data. For an analysis of the higher-order terms in the context of regression, see [5]. Using variational calculus, this action provides the network's average prediction at any point \mathbf{x} in the domain for a general nonlinear operator. Intuitively, one would expect that the effective action follows from taking the continuum limit of $\mathcal{S}[f|X_n]$. Yet doing so is subtle due to the appearance of separate bulk and boundary measures in the continuum limit and the fact that the matrix K^{-1} (unlike K) is measure dependent.

In the next section, using the above effective action, below, we derive the neurally-informed equation for the estimator.

B.2 Derivation of the NIE using variational calculus

Consider a general linear operator of the form L applied to the function, $f(\mathbf{x})$ for $\mathbf{x} \in \mathbb{R}^d$. The effective action for a general operator is as follows,

$$\begin{aligned} \mathcal{S}_{\text{eff}}[f] &= \frac{1}{2}\eta_{\Omega} \int_{\Omega} (Lf(\mathbf{x}) - \phi(\mathbf{x}))^2 d\mathbf{x} + \frac{1}{2}\eta_{\partial\Omega} \int_{\partial\Omega} (f(\mathbf{x}) - g(\mathbf{x}))^2 d\mathbf{x} \\ &\quad + \frac{1}{2} \int_{\Omega} \int_{\Omega} f(\mathbf{x})[K^{-1}](\mathbf{x}, \mathbf{y})f(\mathbf{y})d\mathbf{y}d\mathbf{x}. \end{aligned} \quad (32)$$

Suppose that f_0 is a minimizer, and $h : \Omega \rightarrow \mathbb{R}$ is a variation function,

$$\begin{aligned} \delta\mathcal{S}_{\text{eff}}[f_0] &= \frac{1}{2} \frac{d}{d\epsilon} \mathcal{S}_{\text{eff}}(f_0 + \epsilon h, Lf_0 + \epsilon Lh) \Big|_{\epsilon=0} \\ &= \eta_{\Omega} \int_{\Omega} (Lf_0(\mathbf{x}) + \epsilon Lh(\mathbf{x}) - \phi(\mathbf{x})) Lh(\mathbf{x})d\mathbf{x} \\ &\quad + \eta_{\partial\Omega} \int_{\partial\Omega} (f_0(\mathbf{x}) - \epsilon h(\mathbf{x}) - g(\mathbf{x})) h(\mathbf{x})d\mathbf{x} \\ &\quad + \frac{1}{2} \int_{\Omega} h(\mathbf{x}) \int_{\Omega} [K^{-1}](\mathbf{x}, \mathbf{y}) (f_0(\mathbf{y}) + \epsilon h(\mathbf{y})) d\mathbf{x}d\mathbf{y} \\ &\quad + \frac{1}{2} \int_{\Omega} (f_0(\mathbf{x}) + \epsilon h(\mathbf{x})) \int_{\Omega} [K^{-1}](\mathbf{x}, \mathbf{y}) h(\mathbf{y})d\mathbf{y}d\mathbf{x} \Big|_{\epsilon=0} \\ &= \eta_{\Omega} \int_{\Omega} d\mathbf{x} (Lf_0(\mathbf{x}) - \phi(\mathbf{x})) Lh(\mathbf{x}) \\ &\quad + \eta_{\partial\Omega} \int_{\partial\Omega} (f_0(\mathbf{x}) - g(\mathbf{x})) h(\mathbf{x})d\mathbf{x} \\ &\quad + \int_{\Omega} \int_{\Omega} [K^{-1}](\mathbf{x}, \mathbf{y}) f_0(\mathbf{x}) h(\mathbf{y})d\mathbf{y}d\mathbf{x} \end{aligned} \quad (33)$$

Next, we use our freedom how to parameterize the variation to simplify the boundary terms. Specifically, we consider a variation of the form

$$h(\mathbf{x}) = (K \star \tilde{h})(\mathbf{x}),$$

where \star denote the convolution operator on the bulk measure and $\tilde{h} : \Omega \rightarrow \mathbb{R}$. Note that provided, K , our prior kernel, is invertible, any variation can be presented in this manner. Substituting it Eq. (33),

$$\begin{aligned} \delta\mathcal{S}_{\text{eff}}[f] &= \eta_{\Omega} \int_{\Omega} \int_{\Omega} (Lf_0(\mathbf{x}) - \phi(\mathbf{x})) [LK](\mathbf{x}, \mathbf{y})\tilde{h}(\mathbf{y})d\mathbf{y}d\mathbf{x} \\ &\quad + \eta_{\partial\Omega} \int_{\Omega} \int_{\partial\Omega} (f_0(\mathbf{x}) - g(\mathbf{x})) K(\mathbf{x}, \mathbf{y})\tilde{h}(\mathbf{y})d\mathbf{y}d\mathbf{x} + \int_{\Omega} f_0(\mathbf{x})\tilde{h}(\mathbf{x})d\mathbf{x} \end{aligned} \quad (34)$$

Differentiating with respect to \tilde{h} we have that,

$$\begin{aligned} \eta_{\Omega} \int_{\Omega} (Lf_0(\mathbf{y}) - \phi(\mathbf{y})) [LK](\mathbf{y}, \mathbf{x}) d\mathbf{y} \\ + \eta_{\partial\Omega} \int_{\partial\Omega} (f_0(\mathbf{y}) - g(\mathbf{y})) K(\mathbf{x}, \mathbf{y}) d\mathbf{y} + f_0(\mathbf{x}) = 0 \end{aligned} \quad (35)$$

We note by passing that the above derivation can also be done for a nonlinear operator, by allowing the functional derivative to also act on the operator L .

C Generating some NNGP kernels

The kernel used in the toy model could be generated using the following random neural network acting on a one-dimensional input x

$$f(x) = \sum_{c=1}^C a_c \cos(w_c x) \quad (36)$$

with

$$\begin{aligned} a_c &\sim N(0, \sigma_a^2/C) \\ w_c &\sim N(0, \sigma_w^2) \end{aligned} \quad (37)$$

where we will soon take $\sigma_w^2 = 1/l^2$ and $\sigma_a^2 = \frac{1}{\sqrt{2\pi}l^2}$. The NNGP kernel is then

$$\begin{aligned} K(x, y) &\equiv \langle f(x)f(y) \rangle_{a,w} = \sigma_a^2 \frac{1}{\sqrt{2\pi}\sigma_w^2} \int dw e^{-\frac{w^2}{2\sigma_w^2}} \cos(wx) \cos(wy) \\ &= \frac{\sigma_a^2}{2\sqrt{2\pi}\sigma_w^2} \int dw e^{-\frac{w^2}{2\sigma_w^2}} [e^{iw(x+y)} + e^{iw(x-y)}] = \frac{\sigma_a^2}{2} [e^{-\frac{\sigma_w^2(x+y)^2}{2}} + e^{-\frac{\sigma_w^2(x-y)^2}{2}}] \end{aligned} \quad (38)$$

hence, as mentioned, choosing $\sigma_w^2 = 1/l^2$ and $\sigma_a^2 = 1/\sqrt{2\pi}l^2$ reproduces the desired NNGP kernel. This means that training such a neural network with weight decay proportional to l^2 on the w_c weights, PINN loss, and using Langevin type training, samples from the GP posterior we used in our toy example.

D Green's function for the toy model

We first focus on inverting the bulk operator on the l.h.s. $(K^{-1} - \eta_{\Omega}\delta(x-y)\partial_y^2)$, which now derive. Consider the following set of basis functions for the positive half-interval,

$$\langle x|k > 0 \rangle = \frac{\sqrt{2}}{\sqrt{\pi}} \cos(kx) = \frac{1}{\sqrt{2\pi}} [e^{ikx} + e^{-ikx}] \quad (39)$$

Notably

$$\begin{aligned}
\langle k|k' \rangle &= \int_0^\infty dx \langle k|x \rangle \langle x|k' \rangle \\
&= \int_0^\infty dx \frac{2}{\pi} \cos(kx) \cos(k'x) = \int_{-\infty}^\infty dx \frac{1}{\pi} \cos(kx) \cos(k'x) \\
&= \int_{-\infty}^\infty dx \frac{1}{4\pi} [e^{ikx} + e^{-ikx}] [e^{ik'x} + e^{-ik'x}] = \delta(|k| - |k'|)
\end{aligned} \tag{40}$$

Consider $K(x, y)$ on this basis

$$\begin{aligned}
K|k \rangle &= \int_0^\infty dy K(x, y) \frac{\sqrt{2}}{\sqrt{\pi}} \cos(ky) = \int_{-\infty}^\infty dy K(x, y) \frac{1}{\sqrt{2\pi}} \cos(ky) \\
&= \int_{-\infty}^\infty dy K(x, y) \frac{1}{2\sqrt{2\pi}} [e^{iky} + e^{-iky}] = 2e^{-(kl)^2/2} \frac{1}{\sqrt{2\pi}} \cos(kx) = e^{-(kl)^2/2} |k \rangle
\end{aligned} \tag{41}$$

Transforming the bulk operator to this “ k -space”

$$\langle k|[K^{-1} - \eta_\Omega \partial_x^2]|k' \rangle = \delta(k - k') \left[e^{(kl)^2/2} + \eta_\Omega k^2 \right]. \tag{42}$$

We thus find the following expression for the Green function which is defined here as $[K^{-1} + \eta_\Omega L^T L]G(x, y) = \delta(x - y)$,

$$\begin{aligned}
G(x, x') &= \frac{2}{\pi} \int_0^\infty dk dk' \cos(kx) \cos(k'x') \delta(k - k') \left[e^{+(kl)^2/2} + \eta_\Omega k^2 \right]^{-1} \\
&= \frac{2}{\pi} \int_0^{+\infty} dk \cos(kx) \cos(kx') \left[e^{+(kl)^2/2} + \eta_\Omega k^2 \right]^{-1} \\
&= \frac{1}{\pi} \int_{-\infty}^{+\infty} dk \cos(kx) \cos(kx') \left[e^{+(kl)^2/2} + \eta_\Omega k^2 \right]^{-1} \\
&= \frac{1}{4\pi} \int_{-\infty}^{+\infty} dk [e^{ikx} + e^{-ikx}] [e^{ikx'} + e^{-ikx'}] \left[e^{+(kl)^2/2} + \eta_\Omega k^2 \right]^{-1}.
\end{aligned} \tag{43}$$

This integral can be evaluated numerically or via contour integration. Considering the latter, one finds an infinite set of simple poles. As $|x - x'|$ grows or for very large η_Ω , we find numerically that a single pole dominates the result and yields $G(x, x') \approx \frac{\kappa}{2} \left[e^{-\kappa|x-x'|} + e^{-\kappa|x+x'|} \right]$ where $\kappa = \frac{1}{\sqrt{l^2/2 + \eta_\Omega}}$ for $\kappa l \ll 1$. While this approximation can be systematically improved by accounting for additional poles, in the numerics carried below we simply calculate this integral numerically.

E Deriving the $Q_n[\phi, g]$ figure of merit

Here, we derive the $Q_n[\phi, g]$ figure of merit, which also exposes some hidden algebraic relations between the GPR formula and the neurally-informed equation.

First, we note that one can re-rewrite the neurally-informed equation as an operator equation without performing any integration by parts, namely

$$\int_{\Omega} [K^{-1} + \eta_{\partial\Omega}\delta\delta + \eta_{\Omega}L^{\dagger}L]_{\mathbf{x}\mathbf{y}} f(\mathbf{y}) d\mathbf{y} = \eta_{\partial\Omega}\delta_{\partial\Omega}(\mathbf{x})g(\mathbf{x}) + \eta_{\Omega}L^{\dagger}\phi(\mathbf{x}) \quad (44)$$

where $\delta_{\partial\Omega}(\mathbf{x}) = \int_{\partial\Omega} \delta(\mathbf{x} - \mathbf{z})d\mathbf{z}$, $[\delta\delta]_{\mathbf{x}\mathbf{y}} = \int_{\partial\Omega} \delta(\mathbf{x} - \mathbf{z})\delta(\mathbf{z} - \mathbf{y})d\mathbf{z}$, and $[fL^{\dagger}]_{\mathbf{x}} = [Lf]_{\mathbf{x}}$, which is then consistent with $\int_{\Omega} [L^{\dagger}L]_{\mathbf{x}\mathbf{y}} f(\mathbf{y}) d\mathbf{y} = \int_{\Omega} L^{\dagger}_{\mathbf{x}}\delta(\mathbf{x} - \mathbf{y})L_{\mathbf{y}}f(\mathbf{y})d\mathbf{y}$. Noting that the operator on the l.h.s. is a sum of positive semi-definite operators and that K^{-1} is positive definite (indeed K is generically semi-definite and bounded), we invert the operator on the left-hand side and obtain

$$\begin{aligned} f(\mathbf{x}) &= \eta_{\partial\Omega} \int_{\partial\Omega} [[K^{-1} + \eta_{\Omega}L^{\dagger}L + \eta_{\partial\Omega}\delta\delta]^{-1}]_{\mathbf{x}\mathbf{z}} g(\mathbf{z}) d\mathbf{z} \\ &\quad + \eta_{\Omega} \int_{\Omega} [[K^{-1} + \eta_{\Omega}L^{\dagger}L + \eta_{\partial\Omega}\delta\delta]^{-1}]_{\mathbf{x}\mathbf{y}} [L^{\dagger}\phi]_{\mathbf{y}} d\mathbf{y} \end{aligned} \quad (45)$$

where the inverse is taken with respect to the bulk measure. Next, we define the following operator,

$$\begin{aligned} \hat{K}_{\mathbf{x}\mathbf{y}} &\equiv [[K^{-1} + \eta_{\partial\Omega}\delta\delta]^{-1}]_{\mathbf{x}\mathbf{y}} \\ &= K(\mathbf{x}, \mathbf{y}) - \int_{\partial\Omega} \int_{\partial\Omega} K(\mathbf{x}, \mathbf{z}_1)[K + \eta_{\partial\Omega}^{-1}]^{-1}(\mathbf{z}_1, \mathbf{z}_2)K(\mathbf{z}_2, \mathbf{y})d\mathbf{z}_1d\mathbf{z}_2 \end{aligned} \quad (46)$$

where the second transition is since the operator K is assumed invertible, a Woodbury-type manipulation can be applied. Note also that the inverse after the second inequality is w.r.t. the boundary measure and $\eta_{\partial\Omega} = n_{\partial\Omega}/\sigma_{\partial\Omega}^2$. If the boundary is a single point, obtaining \hat{K} is again straightforward, since the operator inverse becomes just a simple algebraic inverse. Substituting Eq. (46)

$$[K^{-1} + \eta_{\partial\Omega}\delta\delta + \eta_{\Omega}L^{\dagger}L]^{-1} = [\hat{K}^{-1} + \eta_{\Omega}L^{\dagger}L]^{-1}. \quad (47)$$

Next, we perform a similar manipulation to the one leading to \hat{K} namely

$$\begin{aligned} [\hat{K}^{-1} + \eta_{\Omega}L^{\dagger}L]^{-1} &= \hat{K}[1 + \eta_{\Omega}L^{\dagger}L\hat{K}]^{-1} \\ &= \hat{K} - \hat{K}L^{\dagger} \left(\eta_{\Omega}^{-1} + L\hat{K}L^{\dagger} \right)^{-1} L\hat{K} \end{aligned} \quad (48)$$

To obtain the result in the main text, we apply the operator L on Eq. (45), i.e.

Lf . It has two contributions, we first start with the source term contribution

$$\begin{aligned}
& \eta_{\Omega} L \int_{\Omega} \left[[\hat{K}^{-1} + \eta_{\Omega} L^{\dagger} L]^{-1} \right]_{\mathbf{x}\mathbf{y}} [L^{\dagger} \phi]_{\mathbf{y}} d\mathbf{y} \tag{49} \\
&= \eta_{\Omega} L \left[\hat{K} - \hat{K} L^{\dagger} \left(\eta_{\Omega}^{-1} + L \hat{K} L^{\dagger} \right)^{-1} L \hat{K} \right] L^{\dagger} \phi \\
&= \eta_{\Omega} \left[(L \hat{K} L^{\dagger}) - (L \hat{K} L^{\dagger}) \left(\eta_{\Omega}^{-1} + (L \hat{K} L^{\dagger}) \right)^{-1} (L \hat{K} L^{\dagger}) \right] \phi \\
&= \eta_{\Omega} \left[\eta_{\Omega}^{-1} \left(\eta_{\Omega}^{-1} + (L \hat{K} L^{\dagger}) \right)^{-1} (L \hat{K} L^{\dagger}) \right] \phi \\
&= \left(\eta_{\Omega}^{-1} + (L \hat{K} L^{\dagger}) \right)^{-1} (L \hat{K} L^{\dagger}) \phi,
\end{aligned}$$

where to simplify the notation in places where there is no indication of position the position is \mathbf{x} . Similarly, the boundary contribution,

$$\begin{aligned}
& \eta_{\partial\Omega} L \int_{\partial\Omega} \left[[\hat{K}^{-1} + \eta_{\Omega} L^{\dagger} L]^{-1} \right]_{\mathbf{x}\mathbf{z}} g(\mathbf{z}) d\mathbf{z} \tag{50} \\
&= \eta_{\partial\Omega} L \left[\hat{K} - \hat{K} L^{\dagger} \left(\eta_{\Omega}^{-1} + L \hat{K} L^{\dagger} \right)^{-1} L \hat{K} \right] g \\
&= \eta_{\partial\Omega} \left[(L \hat{K}) - (L \hat{K} L^{\dagger}) \left(\eta_{\Omega}^{-1} + (L \hat{K} L^{\dagger}) \right)^{-1} (L \hat{K}) \right] g \\
&= \eta_{\partial\Omega} \left[1 - (L \hat{K} L^{\dagger}) \left(\eta_{\Omega}^{-1} + (L \hat{K} L^{\dagger}) \right)^{-1} \right] L \hat{K} g \\
&= \frac{\eta_{\partial\Omega}}{\eta_{\Omega}} \left(\eta_{\Omega}^{-1} + (L \hat{K} L^{\dagger}) \right)^{-1} L \hat{K} g \\
&= \frac{\eta_{\partial\Omega}}{\eta_{\Omega}} \int_{\partial\Omega} \left[\left(\eta_{\Omega}^{-1} + (L \hat{K} L^{\dagger}) \right)^{-1} L \hat{K} \right]_{\mathbf{x}\mathbf{z}} g(\mathbf{z}) d\mathbf{z}
\end{aligned}$$

Consequently, $Lf - \phi$ is

$$\begin{aligned}
Lf(\mathbf{x}) - \phi &= \left[\left(\eta_{\Omega}^{-1} + (L \hat{K} L^{\dagger}) \right)^{-1} (L \hat{K} L^{\dagger}) - 1 \right] \phi + \frac{\eta_{\partial\Omega}}{\eta_{\Omega}} \left(\eta_{\Omega}^{-1} + (L \hat{K} L^{\dagger}) \right)^{-1} L \hat{K} g \tag{51} \\
&= -\eta_{\Omega}^{-1} \left(\eta_{\Omega}^{-1} + L \hat{K} L^{\dagger} \right)^{-1} \phi + \frac{\eta_{\partial\Omega}}{\eta_{\Omega}} \left(\eta_{\Omega}^{-1} + (L \hat{K} L^{\dagger}) \right)^{-1} L \hat{K} g
\end{aligned}$$

we thus find that $\eta_{\partial\Omega} L \hat{K} g$ acts as an additional source term. While it may seem it diverges with $\eta_{\partial\Omega}$ we recall that \hat{K} goes to zero at this limit for arguments on the boundary, hence its contribution is finite and the overall η_{Ω}^{-1} ensures this quantity $Lf - \phi$ goes to zero. Changing the basis to the eigenfunction basis of $L \hat{K} L^{\dagger}$ leads to the spectral bias result of the main text.

Last, we note by passing that \hat{K} as the interpretation of the dataset-averaged posterior covariance, given that one introduced only boundary points and fixes them to zero [5]. Thus, as $n_{\partial\Omega} \rightarrow \infty$, \hat{K} involving any boundary point, is zero.

From a practical point of view, one can obtain an estimate for \hat{K} at small, $\eta_{\partial\Omega}$. A straightforward expansion of this quantity to its leading order is then,

$$\begin{aligned} \hat{K}_{\mathbf{x}\mathbf{y}} &= K(\mathbf{x}, \mathbf{y}) - \eta_{\partial\Omega} \int_{\partial\Omega} K(\mathbf{x}, \mathbf{z})K(\mathbf{z}, \mathbf{y})d\mathbf{z} \\ &\quad - \eta_{\partial\Omega}^2 \int_{\partial\Omega} K(\mathbf{x}, \mathbf{z})K(\mathbf{z}, \mathbf{z}')K(\mathbf{z}', \mathbf{y})d\mathbf{z}d\mathbf{z}' + O(\eta_{\partial\Omega}^3) \end{aligned} \quad (52)$$

which can then be evaluated also analytically in some cases.

References

- [1] Yasaman Bahri, Ethan Dyer, Jared Kaplan, Jaehoon Lee, and Utkarsh Sharma. Explaining scaling laws of neural network generalization, 2022.
- [2] Tom Brown, Benjamin Mann, Nick Ryder, Melanie Subbiah, Jared D Kaplan, Prafulla Dhariwal, Arvind Neelakantan, Pranav Shyam, Girish Sastry, Amanda Askell, et al. Language models are few-shot learners. *Advances in neural information processing systems*, 33:1877–1901, 2020.
- [3] Shengze Cai, Zhiping Mao, Zhicheng Wang, Minglang Yin, and George Em Karniadakis. Physics-informed neural networks (pinns) for fluid mechanics: A review. *Acta Mechanica Sinica*, 37(12):1727–1738, 2021.
- [4] Abdulkadir Canatar, Blake Bordelon, and Cengiz Pehlevan. Spectral bias and task-model alignment explain generalization in kernel regression and infinitely wide neural networks. *Nature communications*, 12(1):2914, 2021.
- [5] Omry Cohen, Or Malka, and Zohar Ringel. Learning curves for over-parametrized deep neural networks: A field theory perspective. *Physical Review Research*, 3(2):023034, 2021.
- [6] Emilio Jose Rocha Coutinho, Marcelo Dall’Aqua, Levi McClenny, Ming Zhong, Ulisses Braga-Neto, and Eduardo Gildin. Physics-informed neural networks with adaptive localized artificial viscosity. *Journal of Computational Physics*, page 112265, 2023.
- [7] Salvatore Cuomo, Vincenzo Schiano Di Cola, Fabio Giampaolo, Gianluigi Rozza, Maziar Raissi, and Francesco Piccialli. Scientific machine learning through physics-informed neural networks: Where we are and what’s next. *Journal of Scientific Computing*, 92(3):88, 2022.
- [8] Sourav Das and Solomon Tesfamariam. State-of-the-art review of design of experiments for physics-informed deep learning. *arXiv preprint arXiv:2202.06416*, 2022.
- [9] Tim De Ryck and Siddhartha Mishra. Generic bounds on the approximation error for physics-informed (and) operator learning. *Advances in Neural Information Processing Systems*, 35:10945–10958, 2022.

- [10] Olga Fuks and Hamdi A Tchelepi. Limitations of physics informed machine learning for nonlinear two-phase transport in porous media. *Journal of Machine Learning for Modeling and Computing*, 1(1), 2020.
- [11] Adrià Garriga-Alonso, Carl Edward Rasmussen, and Laurence Aitchison. Deep convolutional networks as shallow gaussian processes. *arXiv preprint arXiv:1808.05587*, 2018.
- [12] Tamara G Grossmann, Urszula Julia Komorowska, Jonas Latz, and Carola-Bibiane Schönlieb. Can physics-informed neural networks beat the finite element method? *arXiv preprint arXiv:2302.04107*, 2023.
- [13] Craig M Hamel, Kevin N Long, and Sharlotte LB Kramer. Calibrating constitutive models with full-field data via physics informed neural networks. *Strain*, 59(2):e12431, 2023.
- [14] Boris Hanin and Alexander Zlokapa. Bayesian interpolation with deep linear networks. *Proceedings of the National Academy of Sciences*, 120(23):e2301345120, 2023.
- [15] Zhongkai Hao, Songming Liu, Yichi Zhang, Chengyang Ying, Yao Feng, Hang Su, and Jun Zhu. Physics-informed machine learning: A survey on problems, methods and applications. *arXiv preprint arXiv:2211.08064*, 2022.
- [16] Jiri Hron, Yasaman Bahri, Jascha Sohl-Dickstein, and Roman Novak. Infinite attention: Nngp and ntk for deep attention networks. In *International Conference on Machine Learning*, pages 4376–4386. PMLR, 2020.
- [17] Shudong Huang, Wentao Feng, Chenwei Tang, and Jiancheng Lv. Partial differential equations meet deep neural networks: A survey. *arXiv preprint arXiv:2211.05567*, 2022.
- [18] Arthur Jacot, Franck Gabriel, and Clément Hongler. Neural tangent kernel: Convergence and generalization in neural networks. *Advances in neural information processing systems*, 31, 2018.
- [19] Xiaowei Jin, Shujin Laima, and Hui Li. Physics-enhanced deep learning methods for modelling and simulating flow fields. *Chinese Journal of Theoretical and Applied Mechanics*, 53(10):2616–2629, 2021.
- [20] John Jumper, Richard Evans, Alexander Pritzel, Tim Green, Michael Figurnov, Olaf Ronneberger, Kathryn Tunyasuvunakool, Russ Bates, Augustin Zidek, Anna Potapenko, et al. Highly accurate protein structure prediction with alphafold. *Nature*, 596(7873):583–589, 2021.
- [21] George Em Karniadakis, Ioannis G Kevrekidis, Lu Lu, Paris Perdikaris, Sifan Wang, and Liu Yang. Physics-informed machine learning. *Nature Reviews Physics*, 3(6):422–440, 2021.

- [22] Aditi Krishnapriyan, Amir Gholami, Shandian Zhe, Robert Kirby, and Michael W Mahoney. Characterizing possible failure modes in physics-informed neural networks. *Advances in Neural Information Processing Systems*, 34:26548–26560, 2021.
- [23] Alex Krizhevsky, Ilya Sutskever, and Geoffrey E Hinton. Imagenet classification with deep convolutional neural networks. *Advances in neural information processing systems*, 25, 2012.
- [24] Qianyi Li and Haim Sompolinsky. Statistical mechanics of deep linear neural networks: The backpropagating kernel renormalization. *Physical Review X*, 11(3):031059, 2021.
- [25] Chunyue Lv, Lei Wang, and Chenming Xie. A hybrid physics-informed neural network for nonlinear partial differential equation. *International Journal of Modern Physics C*, 34(06):2350082, 2023.
- [26] Alexander Maloney, Daniel A. Roberts, and James Sully. A Solvable Model of Neural Scaling Laws. *arXiv e-prints*, page arXiv:2210.16859, October 2022.
- [27] Dörthe Malzahn and Manfred Opper. A variational approach to learning curves. *Advances in neural information processing systems*, 14, 2001.
- [28] Stephan Mandt, Matthew D Hoffman, and David M Blei. Stochastic gradient descent as approximate bayesian inference. *arXiv preprint arXiv:1704.04289*, 2017.
- [29] Zhiping Mao, Ameya D Jagtap, and George Em Karniadakis. Physics-informed neural networks for high-speed flows. *Computer Methods in Applied Mechanics and Engineering*, 360:112789, 2020.
- [30] Stefano Markidis. The old and the new: Can physics-informed deep-learning replace traditional linear solvers? *Frontiers in big Data*, page 92, 2021.
- [31] Siddhartha Mishra and Roberto Molinaro. Estimates on the generalization error of physics-informed neural networks for approximating PDEs. *IMA Journal of Numerical Analysis*, 43(1):1–43, 01 2022.
- [32] Rambod Mojjani, Maciej Balajewicz, and Pedram Hassanzadeh. Lagrangian PINNs: A causality-conforming solution to failure modes of physics-informed neural networks. *arXiv preprint arXiv:2205.02902*, 2022.
- [33] Joseph P Molnar, Lakshmi Venkatakrisnan, Bryan E Schmidt, Timothy A Sipkens, and Samuel J Grauer. Estimating density, velocity, and pressure fields in supersonic flows using physics-informed bos. *Experiments in Fluids*, 64(1):14, 2023.

- [34] Gadi Naveh, Oded Ben David, Haim Sompolinsky, and Zohar Ringel. Predicting the outputs of finite deep neural networks trained with noisy gradients. *Physical Review E*, 104(6):064301, 2021.
- [35] Gadi Naveh and Zohar Ringel. *Advances in Neural Information Processing Systems*, 34:21352–21364, 2021.
- [36] Roman Novak, Lechao Xiao, Jaehoon Lee, Yasaman Bahri, Greg Yang, Jiri Hron, Daniel A Abolafia, Jeffrey Pennington, and Jascha Sohl-Dickstein. Bayesian deep convolutional networks with many channels are gaussian processes. *arXiv preprint arXiv:1810.05148*, 2018.
- [37] Guofei Pang and George Em Karniadakis. Physics-informed learning machines for partial differential equations: Gaussian processes versus neural networks. *Emerging Frontiers in Nonlinear Science*, pages 323–343, 2020.
- [38] Ravi G Patel, Indu Manickam, Nathaniel A Trask, Mitchell A Wood, Myoungkyu Lee, Ignacio Tomas, and Eric C Cyr. Thermodynamically consistent physics-informed neural networks for hyperbolic systems. *Journal of Computational Physics*, 449:110754, 2022.
- [39] Maziar Raissi, Paris Perdikaris, and George E Karniadakis. Physics-informed neural networks: A deep learning framework for solving forward and inverse problems involving nonlinear partial differential equations. *Journal of Computational physics*, 378:686–707, 2019.
- [40] Maziar Raissi, Paris Perdikaris, and George Em Karniadakis. Machine learning of linear differential equations using gaussian processes. *Journal of Computational Physics*, 348:683–693, 2017.
- [41] Ruben Rodriguez-Torrado, Pablo Ruiz, Luis Cueto-Felgueroso, Michael Cerny Green, Tyler Friesen, Sebastien Matringe, and Julian Togelius. Physics-informed attention-based neural network for hyperbolic partial differential equations: application to the buckley–leverett problem. *Scientific reports*, 12(1):7557, 2022.
- [42] Matteo Ruggeri, Indradip Roy, Michael J Mueterthies, Tom Gruenwald, and Carlo Scalo. Neural-network-based riemann solver for real fluids and high explosives; application to computational fluid dynamics. *Physics of Fluids*, 34(11), 2022.
- [43] Tim De Ryck, Ameya D. Jagtap, and Siddhartha Mishra. Error estimates for physics informed neural networks approximating the navier-stokes equations, 2023.
- [44] Tim De Ryck, Siddhartha Mishra, and Roberto Molinaro. wpinns: Weak physics informed neural networks for approximating entropy solutions of hyperbolic conservation laws, 2022.

- [45] Inbar Seroussi, Gadi Naveh, and Zohar Ringel. Separation of scales and a thermodynamic description of feature learning in some cnns. *Nature Communications*, 14(1):908, 2023.
- [46] Sifan Wang, Hanwen Wang, and Paris Perdikaris. On the eigenvector bias of fourier feature networks: From regression to solving multi-scale pdes with physics-informed neural networks. *Computer Methods in Applied Mechanics and Engineering*, 384:113938, 2021.
- [47] Sifan Wang, Xinling Yu, and Paris Perdikaris. When and why PINNs fail to train: A neural tangent kernel perspective. *Journal of Computational Physics*, 449:110768, 2022.
- [48] Christopher KI Williams and Carl Edward Rasmussen. *Gaussian processes for machine learning*, volume 2. MIT press Cambridge, MA, 2006.
- [49] Greg Yang, Edward J Hu, Igor Babuschkin, Szymon Sidor, Xiaodong Liu, David Farhi, Nick Ryder, Jakub Pachocki, Weizhu Chen, and Jianfeng Gao. Tuning large neural networks via zero-shot hyperparameter transfer. In A. Beygelzimer, Y. Dauphin, P. Liang, and J. Wortman Vaughan, editors, *Advances in Neural Information Processing Systems*, 2021.